Pitch Oscillation Data and Analysis For a Large HSCT Semispan Wing

Robert C. Scott* and Walter A. Silva,†
Aeroelasticity Branch, NASA Langley Research Center, Hampton, VA 23681

Experimental data from wind-tunnel tests of the Rigid Semispan Model (RSM) performed at NASA Langley's Transonic Dynamics Tunnel (TDT) are presented. The primary focus of the paper is on data obtained from testing of the RSM on the Oscillating Turntable (OTT). The OTT is capable of oscillating models in pitch at various amplitudes and frequencies about mean angles of attack. Steady and unsteady pressure data obtained during testing of the RSM on the OTT is presented and compared to data obtained from previous tests of the RSM on a load balance and on a Pitch and Plunge Apparatus (PAPA). Testing of the RSM on the PAPA resulted in flutter boundaries that were strongly dependent on angle of attack across the Mach number range. Pressure data from all three tests indicates the existence of vortical flows at moderate angles of attack. The correlation between the vortical flows and the unusual flutter boundaries from the RSM/PAPA test is discussed. Comparisons of experimental data with steady and unsteady analyses using the CFL3Dv6 computational fluid dynamics code are presented.

Key words: Aeroelasticity, Unsteady Aerodynamics, Flutter, CFD, CFL3D.

Introduction

A primary goal of the Transonic Dynamics Tunnel (TDT) at the NASA Langley Research Center (LaRC) is to acquire high-quality wind-tunnel data for the validation of aeroelastic analysis methods including the development and application of aeroelastic computational fluid dynamics (CFD) codes. The need for such data has been recognized for many years and has led to the development of various programs to generate a database of high quality unsteady data. The RTO effort[1] is an example of an international cooperative effort to define, compile, and disseminate high-quality experimental data sets. A NASA Langley effort was the Benchmark Models Program (BMP). The BMP resulted in the testing of several configurations for which steady and unsteady pressures and flutter data were obtained.[2–7]

The Rigid Semispan Model (RSM), which is the focus of this paper, and an identically shaped flexible version[8] of the RSM were defined near the end of the BMP. These wind-tunnel models, intended to be representative of a high-speed civil transport (HSCT), became part of the Aeroelasticity element of the High Speed Research (HSR) program.

The objective of the Aeroelasticity element of the HSR program was to provide validated analyses, design tools, and demonstrate technology readiness to accurately predict and solve the aeroelastic problems of an advanced high-speed civil transport (HSCT). As part of this task, a wind-tunnel models subtask was created to measure and document the aeroelastic characteristics, the steady and unsteady pressures and forces, and the aeroelastic stability boundaries for models of increasing complexity. One of the goals of this activity was to perform various tests on the RSM.

The RSM was tested on three different mount systems. These were a 5 degree of freedom (DOF) balance, a 2 DOF Pitch and Plunge Apparatus (PAPA), and a single DOF Oscillating Turntable (OTT). Reference 9 described the OTT database, presented samples of steady and unsteady pressure data, and made comparisons between OTT data and data acquired on previous wind-tunnel tests. In addition, reference 9 presented a limited set of steady CFD results which were compared with experimental data. This paper is a continuation of the work described in reference 9, and it will summarize those findings and present additional steady and unsteady CFD analyses.

Experimental Apparatus

Transonic Dynamics Tunnel

The Langley Transonic Dynamics Tunnel (TDT) is a unique national facility dedicated to identifying, understanding, and solving relevant aeroelastic and aeroservoelastic problems. The TDT is a closed-circuit, continuous-flow, variable-pressure, wind tunnel with a 16-foot square test section with cropped corners. The tunnel uses either air or a heavy gas as the test medium and can operate at stagnation pressures from near vacuum to atmospheric, has a Mach number range from near zero to 1.2 and is capable of maximum Reynolds num-

*Senior Aerospace Engineer, AIAA Senior Member.
†Senior Research Scientist, AIAA Senior Member.

Table 1 Summary of RSM wind-tunnel tests (C=Closed, O=Open).

Test No.	Year	Test Medium	Mount	Fuselage Length	Sidewall Slots	Wing/Fus Gap	Nacelles	Data
499	1994	R-12	BAL	18 ft.	O	O	On/Off	AOA/Flap Polars
508	1995	R-12	BAL	11	O/C	O/C (Foam)	On/Off	AOA/Flap Polars
			PAPA	11	C	C (Foam)	On/Off	Shaker Excitation
513	1995	R-12	BAL	18	O/C	C (Foam)	On/Off	None
520	1996	R-12	BAL	18	O/C	C (Foam)	On/Off	AOA/Flap Polars
530	1998	R-134a	PAPA	14	C	C (Tape)	On/Off	Flutter Boundary
		R-134a	STRUT	14	C	C (Tape)	Off	AOA Polars, Tufts
547	2000	R-134a	OTT	14	C	C (Tape)	Off	Wing Oscillation

Table 2 Pitch oscillation amplitudes ($\alpha_1, \pm$Deg.) acquired for various mean angles of attack (α_o, Deg.) and pitch frequency (f, Hz.) combinations for Test 547 (OTT).

α_o	f=0	f=1	f=2	f=5	f=8	f=10
-5	0	2	1	1	0.5	0.25, 0.5
-3	0	2	1	1	0.5	0.25, 0.5
0	0	2	1	1	0.5	0.25, 0.5
0	0	3	1.5	1.5	1	0.5, 1.0
3	0	2	1	1	0.5	0.25, 0.5
6	0	2	1	1	0.5	0.25, 0.5
9	0	2	1	1	0.5	0.25, 0.5
12	0	2	1	1	0.5	0.25, 0.5
15	0	2	1	1	0.5	0.25, 0.5

bers of about 3 million per foot in air and 10 million per foot in heavy gas. Until 1996, the TDT used dichlorodifluoromethane, R-12, as the heavy gas test medium; since then, for environmental reasons, the TDT has used 1,1,1,2 tetrafluoroethane, R-134a.[10,11]

Rigid Semispan Model (RSM)

The RSM planform is a 1/12th scale configuration based on an early HSCT design known as the Reference H configuration. Model airfoil shapes were based on those of the Reference H, with the model wing thickness being increased to a constant 4% thickness-to-chord ratio in order to accommodate pressure instrumentation at the wing tip. The model was designed to be very stiff to allow the measurement of aerodynamic properties without the effects of structural deformations.

Figure 1 shows the planform layout and main components of the RSM including the three primary mounts used during the various wind-tunnel tests. The leading and trailing edges were removable in order to access pressure instrumentation in those regions. A removable tip cap allowed access to pressure instrumentation at the wing tip. The RSM could be tested either with or without a pair of flow-through nacelles. The nacelles were rigidly attached to pylons on the lower, inboard surface

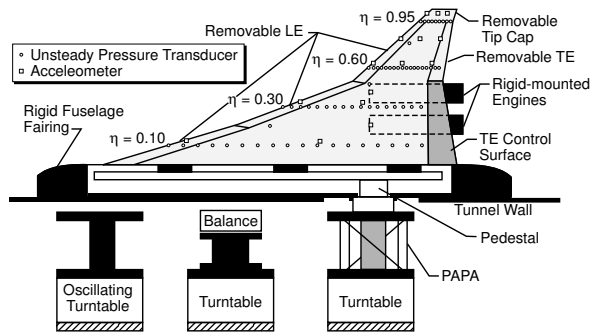

Fig. 1 Planform, model details, and instrumentation layout for the RSM wind-tunnel model.

of the wing. The RSM wing had a graphite epoxy composite structure with an open-cell foam core. The RSM was re-built in 1995 after experiencing a failure of the bond of the upper and lower surfaces. Rivets were inserted along the front and rear spars to eliminate the possibility of a similar failure in future testing, and the original four-pound (i.e. a density of 4 lb/ft^3) foam core was replaced with an eight-pound foam core for added strength and durability.

The RSM was tested with a rigid fuselage fairing which displaced the model away from the wind-tunnel wall boundary layer while serving as an aerodynamic boundary condition at the wing root. Additionally, the rigid fuselage fairing provided an aerodynamic shield for the hardware, instrumentation, and wire bundles located at the wing root. Three different fuselage fairings were used with the RSM. The lengths of these fuselage fairings were approximately 18, 14, and 11 feet. The 18 and 11-foot fuselages had a near rectangular cross-section with rounded corners while the 14-foot fuselage was approximately semi-circular. The aft ends of the 18 and 11-foot fuselages were rather blunt, while the 14-foot fuselage extended further downstream with a more gradual taper to reduce turbulence near the trailing edge of the wing. The center of rotation for the 18 and 11-foot fuselages was 142 inches aft of a reference point defined by the leading edge of the 18-foot fuselage. The center

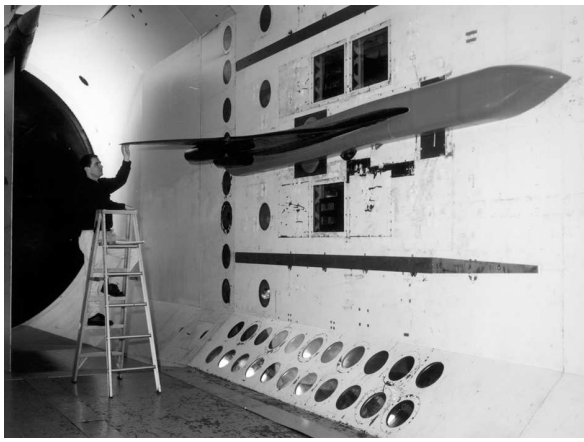

Fig. 2 The RSM and 18 foot fuselage mounted in the TDT test section.

of rotation for the 14-foot fuselage was 133 inches aft of this point. This resulted in the wing center of rotation being moved 9 inches forward when installed on the 14-foot fuselage. A photograph of the RSM, engine nacelles, and the 18-foot long fuselage fairing installed in the TDT test section is shown in figure 2.

The instrumentation layout for the RSM (visible in figure 1) consisted of 131 insitu unsteady pressure transducers located at the 10, 30, 60, and 95% span stations. Six additional unsteady pressure transducers were installed at the 20% chord station for the 20, 45, and 75% span stations for both upper and lower surfaces. Channels were carved into the foam core to accommodate the wiring for the instrumentation. Instrumentation also included accelerometers installed throughout the wing. The 18 and 11-foot long fuselage fairings were instrumented with 120 steady pressure orifices at seven fuselage stations. The 14-foot long fuselage fairing was instrumented with unsteady pressure transducers.

Balance

A five-degree-of-freedom sidewall balance was used for the measurement of loads on the RSM. The loads measured were for the wing alone and not for the combined wing/fuselage fairing configuration. Measurement of the combined wing/fuselage fairing loads would have impeded computational validation efforts since the quality of the data would have been compromised by the complex interaction of the fuselage with the tunnel wall boundary layer. In addition, loads data from a combined wing/fuselage fairing configuration is of questionable value since it is impossible to discern the contribution of each component (wing or fuselage) from the measured load, again, impeding validation efforts. For these reasons, the wing was attached to the balance but the fuselage fairing was not. The wing/balance system and the fuselage fairing were attached to the tunnel turntable

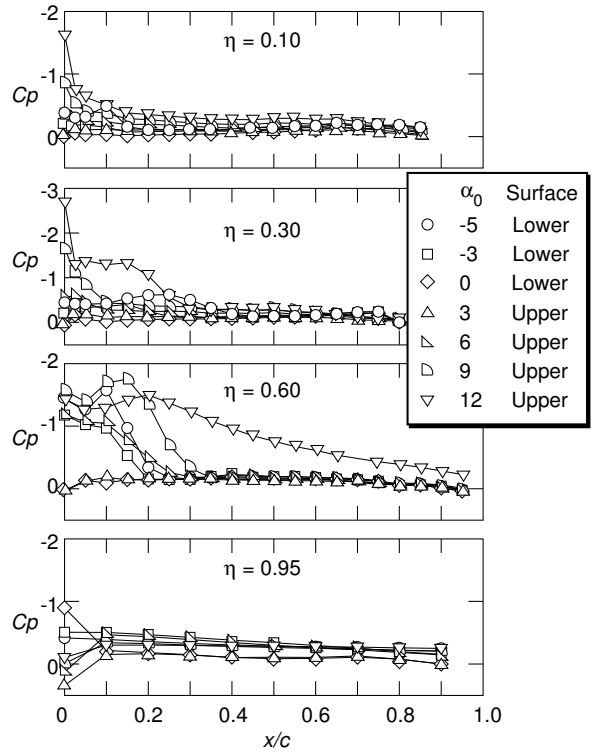

Fig. 3 Comparison of Test 547 (OTT) steady pressure coefficients (suction side only) for seven mean angles of attack. M=0.50 and q=150 psf.

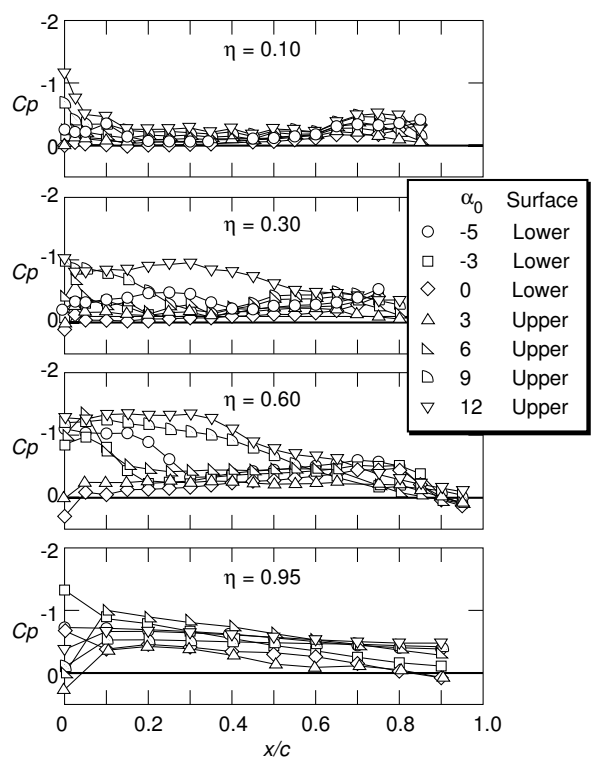

Fig. 4 Comparison of Test 547 (OTT) steady pressure coefficients (suction side only) for seven mean angles of attack. M=0.95 and q=150 psf.

via independent hardware connections. During one RSM wind-tunnel test a strut was used in place of the balance so data could be acquired at higher angles of attack.

Pitch And Plunge Apparatus (PAPA)

The RSM PAPA mount is an updated version of the PAPA mount used in NASA Langley's Benchmark Models (BMP) program.[2,4–7] The BMP PAPA mount[12] was developed at NASA Langley Research Center, and when used with a rigid model, provides the two flexible degrees of freedom (pitch and plunge) needed for classical flutter. The RSM PAPA is much stiffer than the BMP PAPA so it can accommodate the increased mass, pitch inertia, and aerodynamic forces and moments of the RSM as compared to the BMP models. The BMP PAPA consisted of 4 rods between a fixed and a moving plate, while the RSM PAPA had 8 rods. The rigid-body plunge mode consists of vertical translation of the RSM and the rigid-body pitch mode consists of rotation of the RSM about an axis of rotation, typically the elastic axis of the RSM/PAPA system. Additional design details of the RSM PAPA are available in reference 13.

Oscillating Turntable

The RSM was the first model to be tested using the TDT's new Oscillating Turntable (OTT). The OTT is essentially a very large hydraulic actuator that can be used to oscillate side-wall mounted models at arbitrary pitch angles. The TDT OTT is unique because of its ability to oscillate high inertia models (up to 65,000 lbm-in^2) ± 1 degree at frequencies up to 40 Hz. at transonic conditions. Using the OTT, steady angles of attack and unsteady pitch oscillations can be obtained. Typically, models are oscillated at a prescribed frequency and amplitude about a mean angle of attack. The frequency response of the OTT-plus-model is dependent on model inertia and aerodynamic loads. For the RSM, frequencies in excess of 10 Hz. were demonstrated. Reference 14 contains details of the OTT design and operation.

RSM Wind-Tunnel Tests

Table 1 summarizes key aspects of the six RSM wind-tunnel tests. With the exception of TDT Test 547, all tests were performed as part of NASA's High Speed Research (HSR) program. Personnel from The Boeing Company (one of NASA's partners in the HSR program) participated in the planning and execution of these tests.

The first RSM test (499) was plagued by numerous problems with the model subsystems, but ultimately, the problems were solved and a preliminary aerodynamic database was acquired. Comparison of this data with analysis and data obtained in other wind tunnels indicated some discrepancies. The most notable difference was in the lift-curve slopes. Further study indicated that the likely cause of this discrepancy was the proximity of open slots in the TDT test section wall to the RSM model. These open slots altered the flow over the wing by allowing flow through the wall from the high to the low pressure side.

The original objective of Test 508 was to obtain flutter data requiring the use of the shorter, lower inertia fuselage (11 foot). When it was found that this configuration would not flutter, the test objectives were changed. Test 508 explored the effects of the side-wall slots being open or closed. Additionally, the effects of leaving open and closing gaps between fuselage and wing and between fuselage and test section wall were explored. The fuselage-to-wing gap could be sealed with foam or tape depending on whether the wing loads were being measured. A small gap still existed with the use of foam. CFD results, data obtained in other wind-tunnels, in addition to data from this and the preceding RSM wind-tunnel test indicated that the most appropriate configuration was slots closed and gaps sealed.

The purpose of Test 513 was to use the lessons learned from the preceding tests to acquire a large, high quality, aerodynamic database. Unfortunately, the RSM delaminated before any significant data was acquired. After the model was repaired, Test 520 successfully acquired this aerodynamic data.

The last two tests, 530 and 547, used a new, aerodynamically improved fuselage. Additionally, the new fuselage had a different center of rotation and center of gravity so that RSM/PAPA flutter data could be acquired. Test 530 acquired flutter data with and without engine nacelles. Test 547 acquired data while the model was oscillated on the OTT.

While significant lessons were learned on the first three tests of the RSM, only the last three tests are considered to have been successful in generating quality aerodynamic data for code validation.

RSM Experimental Data

The RSM data acquired during Test 520 (balance) has been thoroughly documented in reference 15. Reference 13 summarizes several HSR tests including RSM Test 530 (PAPA), but it did not examine any of the unsteady aerodynamic data. Additionally, both the balance and PAPA mounts have a limited angle-of-attack range due to load and deflection limits. The larger load limits on the OTT allowed mean angles of attack up to 12 degrees. The focus of this section of the paper will be to document the aerodynamic data acquired during Test 547, including steady pressures and a comparison with some data from Test 520 (bal-

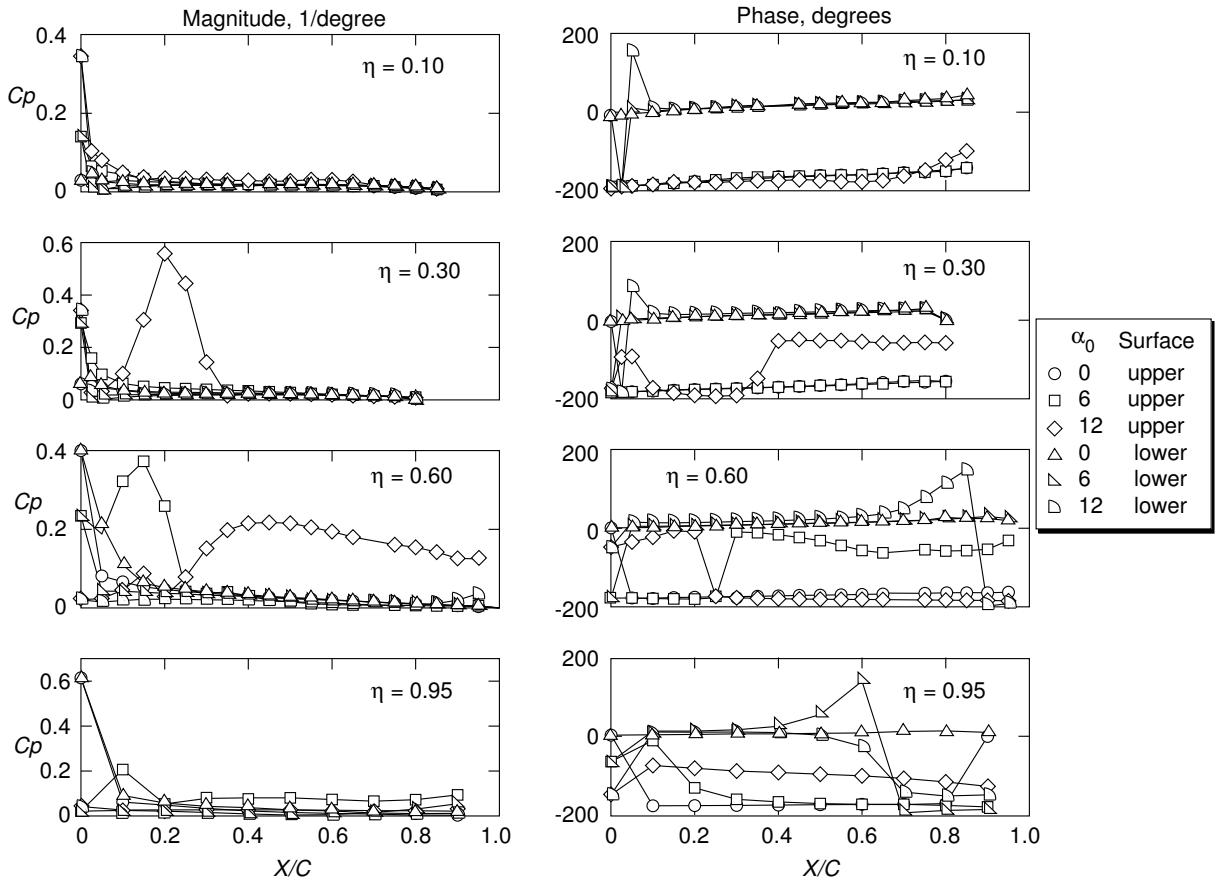

Fig. 5 Comparison of Test 547 (OTT) unsteady pressures at three mean angles of attack. M=0.50, q=150 psf., f_{OTT}=2 Hz., and α_1=±1 deg.

ance). Unsteady pressures from Test 547 will also be examined and, where appropriate, compared with corresponding data from Test 530 (PAPA).

OTT Database Description

The RSM/OTT database is comprised primarily of data acquired at various combinations of two dynamic pressures (q) and ten Mach numbers (M). The dynamic pressures were 100 and 150 psf, and the Mach numbers were 0.5, 0.7, 0.8, 0.9, 0.95, 0.98, 1.0, 1.02, 1.05, and 1.1. Table 2 summarizes the various combinations of mean angle of attack (α_o), pitch oscillation frequency (f_{OTT}), and pitch amplitude (α_1) at which data were acquired. At each combination of M, q, and α_o, a steady data point (i.e. f=0 Hz.) was acquired. The length of each time history was either 15 or 30 seconds depending on the frequency of oscillation. Additionally, at each combination of M and q, data were acquired during a sine sweep from 1 to 12 Hz. Other data acquired during the RSM/OTT wind-tunnel test included M, q, and α_o conditions corresponding to the flutter points obtained from Test 530 (RSM/PAPA).

Steady Data

Figures 3 and 4 show examples of mean pressure coefficients acquired on the OTT at several fixed angles of attack (f=0 Hz.). The data shown in figure 3 is for a subsonic Mach number of 0.5 and all the pressure coefficients are well below C_p critical ($C_{p_{cr}}$=-2.38). Thus, none of the features in the data can be attributed to shock waves. All span stations exhibit a variation of the leading edge suction peak with angle of attack. The most interesting features of this data can be found at 30 and 60% span. Here the effects of vortical flow can be seen at the larger magnitude angles of attack. At 60% span, vortical flow is noted on the lower surface from the leading edge to 20% chord for -5 and -3 degrees, and on the upper surface for angles of 6, 9, and 12 degrees. At this Mach number the zero lift angle of attack for the RSM is approximately 1.6 degrees, and the pressures at the 60% span station display reasonable symmetry with respect to that angle. At 30% span, vortical flow is noted for 12 degrees and to a lesser extent and further aft, vortical flow is shown in the -5 degree data. The 10% span and 95% span stations exhibit no significant features with the exception of the -5 degree data at 10% span. Here, vortical flow appears to be present on the lower surface at 10% chord. The potential significance of this relative to RSM/PAPA flutter will be discussed later.

The data shown in figure 4 was acquired at a

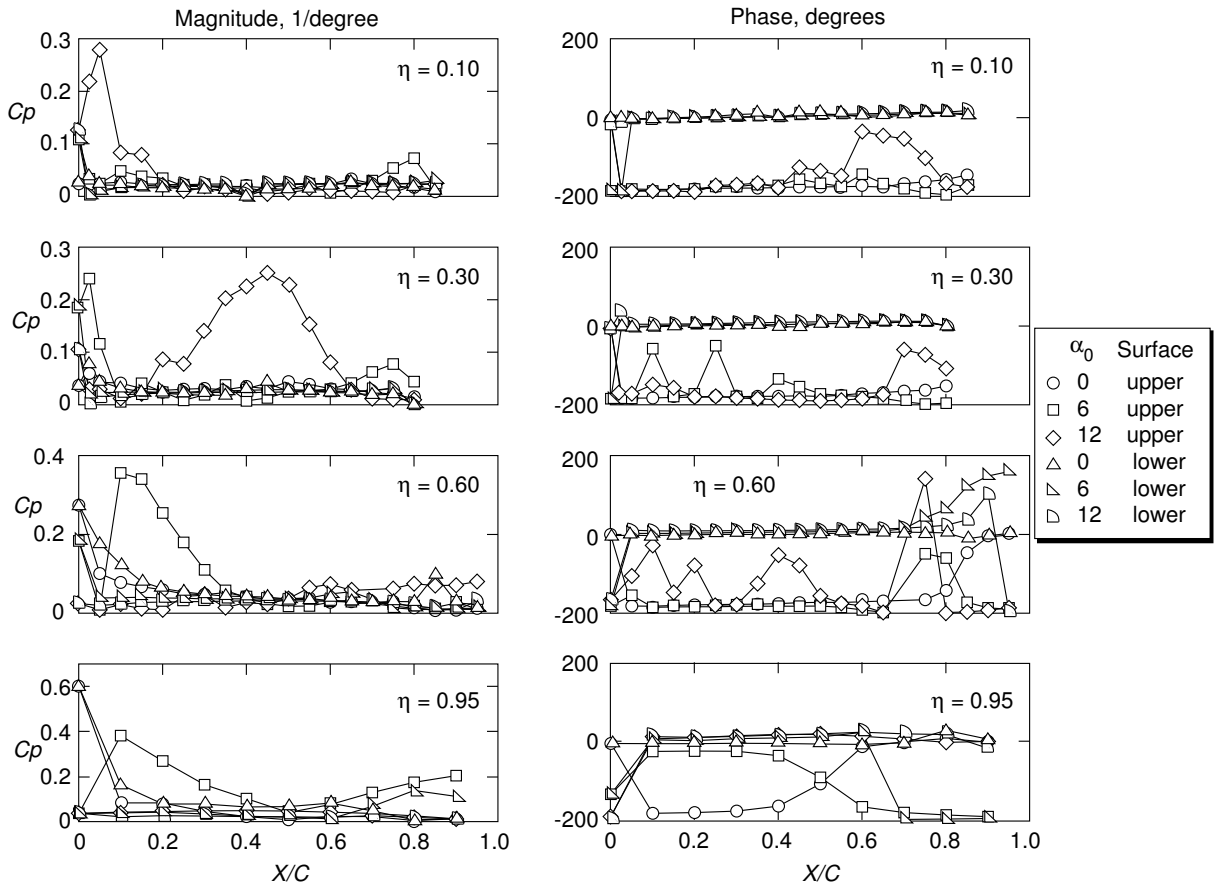

Fig. 6 Comparison of Test 547 (OTT) unsteady pressures at three mean angles of attack. M=0.95, q=150 psf., f_{OTT}=2 Hz., and α_1=±1 deg.

Mach number of 0.95. In general, the major features of this data are very similar to the Mach 0.5 data. The primary difference is that the pressure distributions tend to be flatter. This observation is consistent with the general tendency for the pressure distribution to flatten out with increased Mach number for this type of planform due to the effects of compressibility on the vortex. For this type of configuration, shocks generally occur near the trailing edge of the wing. Although difficult to see in this plot, shocks are present at the 60% span station and 85% chord for some mean angles of attack.

Unsteady Data

Figures 5 and 6 show samples of unsteady pressure data acquired during Test 547 (OTT). Magnitude and phase of C_p at a forced frequency of 2 Hz. and an oscillation amplitude of ±1 degree are shown for three angles of attack at a subsonic and a transonic Mach number. High magnitudes in this type of data are generally associated with shock motion or movement of vortical flow regions. In both sets of data, large magnitudes are noted at the leading edge for the nonzero angles of attack. In the subsonic data, the effects of vortex motion are seen primarily at 30 and 60% span. There may be a small amount of vortex motion near the leading edge at 95% span for 6 degrees, and no vortex motion is noted at 10% span. The transonic data in figure 6 shows many of the same features that were found in the subsonic data. In general, the major features found in the subsonic data are moved further aft in the transonic data. Additionally, several new features are noted near the leading edge for 10 and 30% span. Examination of the data in figure 4 where $C_{p_{cr}}$=-0.1 indicates that these features are probably not associated with shock waves but are also the result of vortical flow. The magnitude peak hinted at in the 95% span, subsonic data is more pervasive at this condition.

Some of the data from Test 530 (PAPA) will now be examined and compared with corresponding data from Test 547 (OTT). The flutter points and boundaries for the RSM/PAPA configuration are shown in figure 7. These results were for a clean wing, but similar results were also found with the engine nacelles installed. Time history data were acquired at each of the flutter points. The results are plotted as dynamic pressure versus Mach number for various values of the mean angles of attack. The baseline (0 degrees) flutter boundary exhibits a shallow transonic dip followed by an abrupt rise. As angle of attack becomes more negative, the

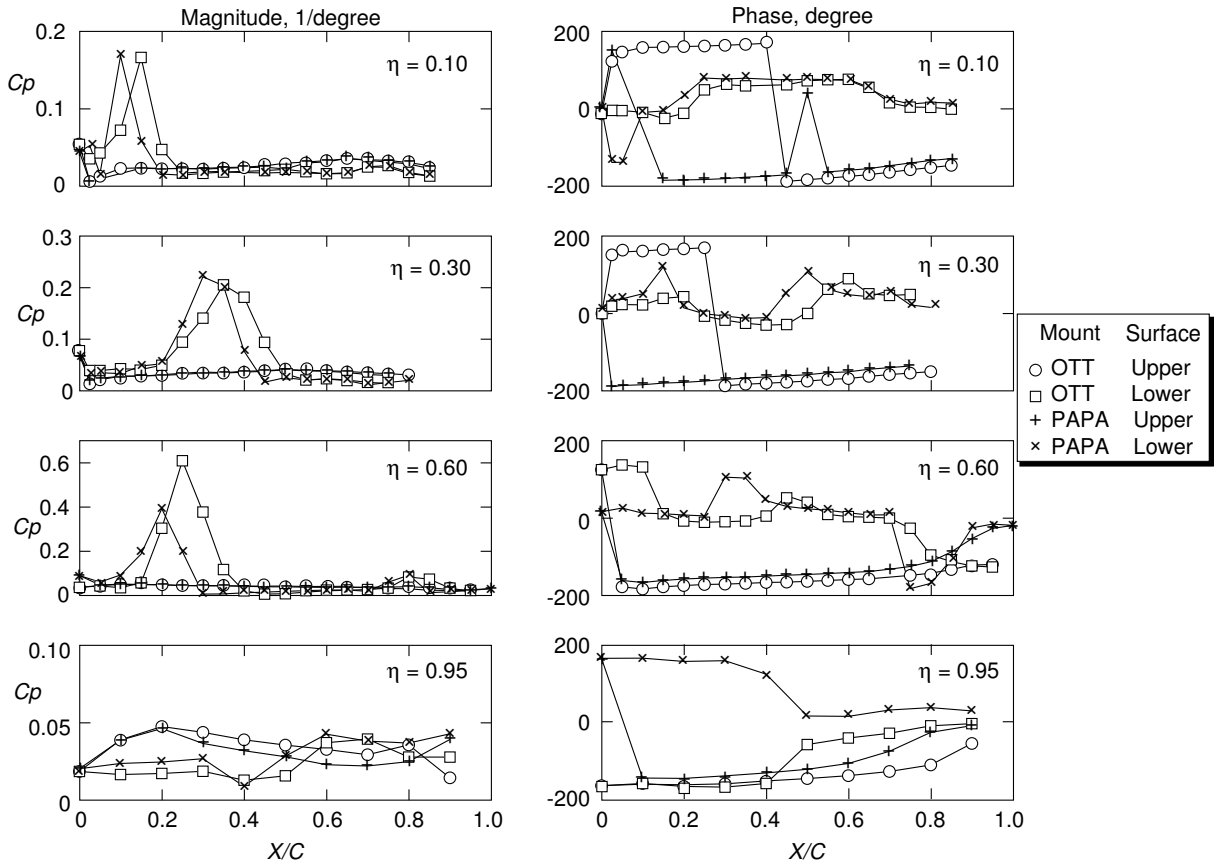

Fig. 8 Comparison of OTT and PAPA unsteady pressure data. M**=0.934,** q**=48 psf,** $\alpha_{o_{OTT}}$**=-5 deg.,** $\alpha_{o_{PAPA}}$**=-4.75 deg.,**f_{OTT}**=4.87 Hz.,** α_1**=±0.5 deg., and** f_{PAPA}**=4.74 Hz.**

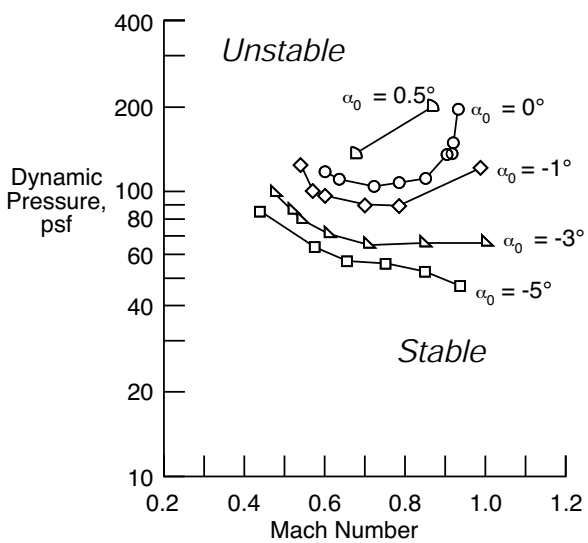

Fig. 7 Experimental flutter boundaries as a function of mean angle of attack for the RSM/PAPA configuration, no nacelles.

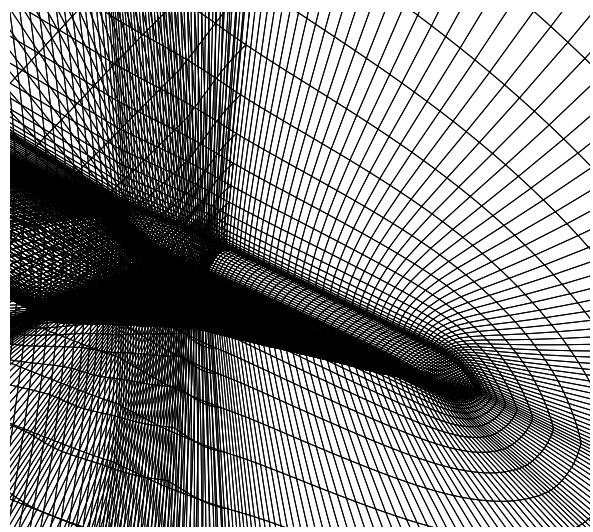

Fig. 9 Computational grid for RSM with 14-foot fuselage.

boundaries shift to lower dynamic pressures and tend to flatten out. The flutter frequency for these results varied from 4.75 to 4.78 Hz. The results presented in figure 7 were unexpected for what was considered a simple 2 degree-of-freedom configuration. The flutter results indicate a strong dependence on angle of attack which is unusual for thin wings at subsonic conditions.

The strong relationship between the flutter boundary and angle of attack may be due in large part to the airfoil shape on the strake portion of the wing. While the outboard wing has a sharp leading edge, the strake portion of the wing has a rounded leading edge but has a relatively flat lower surface. Because of this strake geometry negative angles of attack would have a greater tendency to generate

vortical flow further forward and inboard on the lower surface of the strake than positive angles on the upper surface. This hypothesis is supported by the steady data shown in figure 3 where there is evidence of a lower surface strake vortex at 10% span for -5 degrees angle of attack. For this span station there is no evidence of vortical flow for any of the positive angles up to 12 degrees. Similarly for the 30% span there is evidence of a lower surface strake vortex at -5 and, to a lesser extent, -3 degrees. At this span station, evidence of an upper surface vortex exists only at 12 degrees. The formation of the strake vortex on the lower surface as angle of attack is reduced to -5 degrees would cause the center of pressure to move forward and apparently, had a destabilizing effect on the flutter boundary.

Figure 8 shows a comparison between unsteady pressure data acquired during Test 530 (PAPA) and data acquired at approximately the same flow conditions during Test 547 (OTT). The PAPA data shown is for the Mach 0.93, -5 degrees angle of attack, flutter point shown in figure 7. Here, the OTT data approximately replicates the flow features found in the flutter data. Considering the known differences between the two test conditions, the agreement is very reasonable. While the flutter mode observed on PAPA was dominated by pitching motion, the flutter mode did include a plunging component and the center of rotation was not at the PAPA shear center. In contrast, the OTT data was for pure pitching oscillation about a fixed center of rotation. Another difference was that the amplitude of oscillation for the PAPA data was increasing during data acquisition while the OTT data was acquired for a fixed amplitude oscillation. Finally, there was an angle-of-attack difference due to aeroelastic twist of PAPA. The reported angle of attack for PAPA was measured on the fixed end of the mount.

Examination of all the PAPA flutter data and corresponding OTT data indicate that the best correlation between the two data sets is for -5 degrees angle of attack. For the -3 degree angle-of-attack data (not shown), the 30 and 60% span data generally agree while the 10 and 95% data show poor correlation. The correlation for the -1, 0 and 0.5 degree data is generally poor. One possible explanation for these discrepancies is the difference in angle of attack due to PAPA twist. The key features of the flow are probably not as sensitive to small differences in angle of attack when the magnitude of the angle is large.

CFD Analysis

There is significant interest in using the RSM data, acquired during its various tests, for validating computational methods. A primary reason for this interest is the unusual flutter boundary (figure 7) acquired during testing of the RSM on the PAPA. As previously mentioned, high-aspect ratio wings with thin airfoils exhibit little variation in the flutter dynamic pressure due to moderate changes in angle of attack at subsonic conditions. This characteristic allows the use of linear flutter analysis methods based on lifting surface theories (flat plate models). But the flutter boundary exhibited by the RSM on the PAPA is indicative of significant nonlinear effects since the flutter boundary is a strong function of angle of attack across the Mach number range. Therefore, since there are no shocks at subsonic conditions, the nonlinear effects must be due to vortical flow induced by the RSM's low aspect ratio, high inboard sweep, and outboard sharp leading edge. As a result of this aeroelastic sensitivity to complex flow physics, this data set poses an interesting challenge to the validation of computational methods.

CFL3Dv6 and Grids

The recently-developed CFL3D version 6.0 (CLF3Dv6)[16,17] computational fluid dynamics (CFD) code is being used for the steady and unsteady analysis of the RSM wind-tunnel model. The CFL3Dv6 code solves the time-dependent conservation law form of the Reynolds-averaged Navier-Stokes equations using a finite-volume approach. Upwind-biasing is used for the convective and pressure terms while central differencing is used for the shear stress and heat transfer terms. Implicit time advancement is used with the ability to solve steady or unsteady flows. Subiteration and multigrid capabilities are available for improved accuracy and convergence acceleration. In addition, numerous turbulence models are provided. In this paper, all results were computed using the Spalart-Allmaras turbulence model.

Data from photogrammetry, used to measure surface ordinates, was used to generate IGES models of the RSM and the 14-foot fuselage. These IGES models were then used to create grids for subsequent use in CFD analyses. One such grid is shown in figure 9. It is a C-H topology grid dimensioned 305x81x49 grid points, suitable for Navier-Stokes calculations. A somewhat more refined 361x89x49 grid was also used in this analysis. These grids will be referred to as grid 1 and grid 2, respectively.

Steady Computational Results and Comparisons with Experimental Data

Reference 9 presented a comparison of computational and experimental steady pressure distributions at a Mach number of 0.95, Re=2.2×10^6/ft, and α_o=6, 3, -3, and -5 degrees using grid 1. These calculations have since been repeated using grid 2. In addition, computations were also performed at

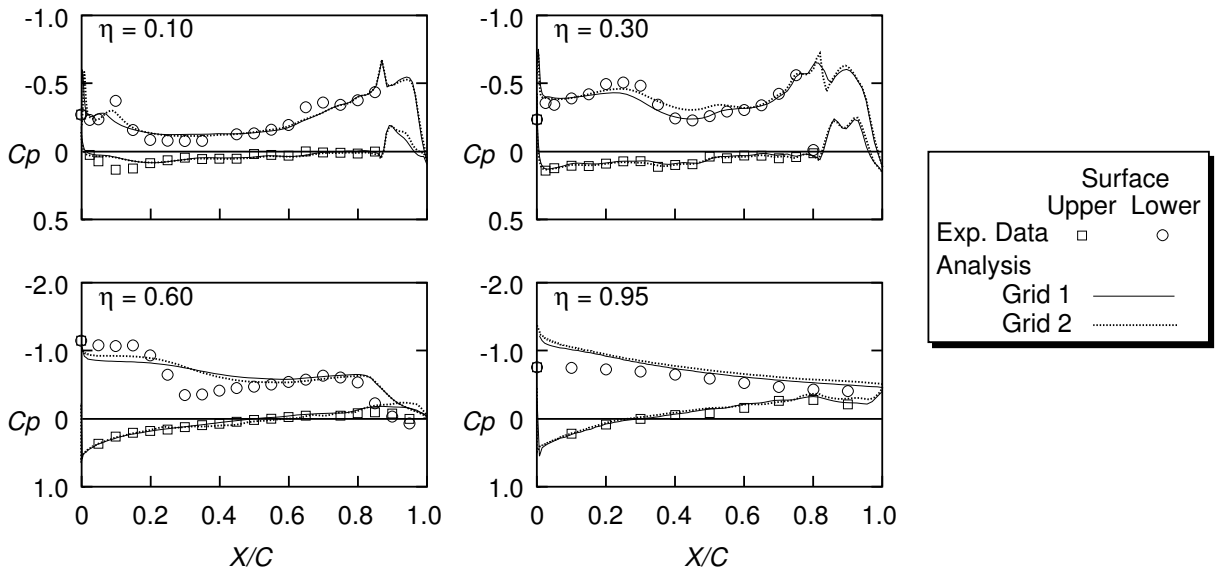

Fig. 10 Comparison of CFL3D analysis and Test 547 (RSM/OTT) steady pressure coefficients. M=0.95, q=150 psf, Re=2.2×10^6/ft, and α_o=-5 deg.

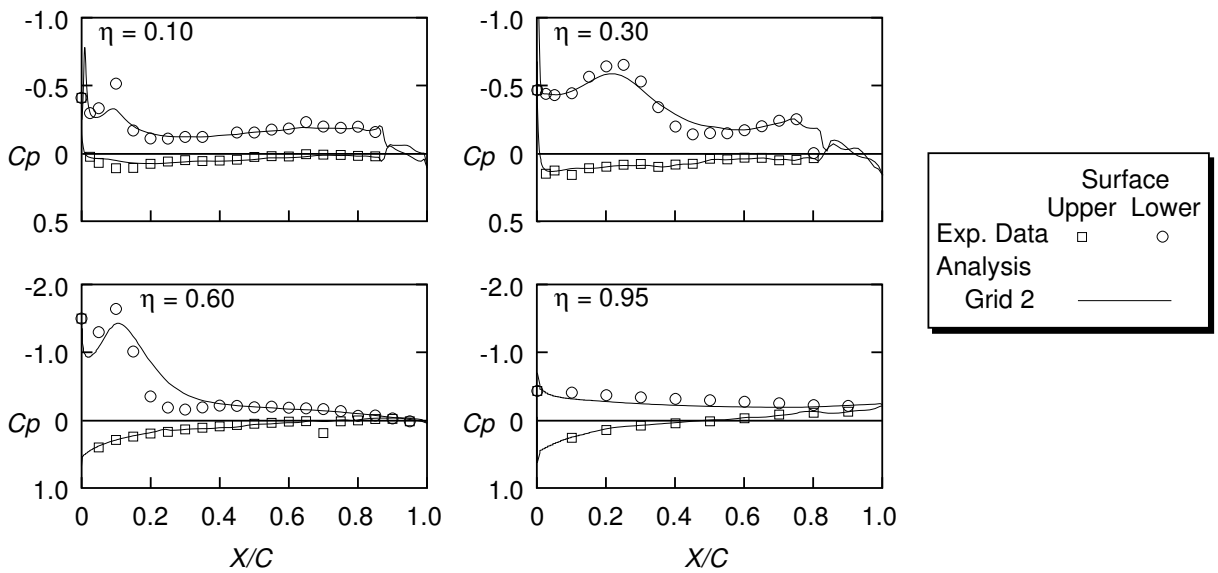

Fig. 11 Comparison of CFL3D analysis and Test 547 (RSM/OTT) steady pressure coefficients. M=0.5, q=150 psf, Re=4.3×10^6/ft, and α_o=-5 deg.

a Mach number of 0.5, Re=4.3×10^6/ft, and α_o=6, 3, -3, and -5 degrees using grid 2. This section will summarize the status of the steady calculations.

The steady Mach 0.95 calculations described in reference 9 showed generally good correlation between analysis using grid 1 and the experimental data for α_o=6, 3, -3, and -5 degrees. Differences between the experimental and analytical data were generally associated with vortical flow on the suction side of the wing. It was felt that improved grid resolution may be needed for the outboard span stations in order to capture the vortical flow phenomena.[18] Grid 2 was developed in an attempt to improved the steady correlation prior to performing unsteady calculations. Comparisons of the grid 1 and grid 2 calculations and experimental data for the four angles of attack indicate that the computation results are generally improved in the vicinity of the vortical flow by the use of grid 2.

Figure 10 shows a comparison between the grid 1 and grid 2 calculations and experimental data for a Mach number of 0.95 at -5 degrees angle of attack. The large variations in the computational results at the 10 and 30% span stations near the trailing edge are due to surface variations associated with the trailing edge control surface. The control surface was not instrumented with pressure ports so there are no pressure measurements available for this region. Evidence of vortical flow can be seen near the leading edge at the 10, 30, and 60% span stations in both the analytical and experimental data. As indicated by the dashed line, the correla-

tion is improved at all three span stations by the use of grid 2. Unfortunately, the grid resolution is still inadequate to fully capture the vortex at 60% span. The correlation of analytical data was not improved in the vicinity of the wing tip (95% span) by the use of grid 2.

Calculations using grid 2 were performed at a Mach number of 0.5 and α_o=6, 3, -3, and -5 degrees. In general, the correlation between analysis and experimental data is somewhat better than the Mach 0.95 comparisons discussed previously. All major flow features appear to be captured with the exception of a mild vortex at 10% span and α_o= -3 degrees. Figure 11 shows a comparison between the grid 2 calculations and experimental data for a Mach number of 0.5 at -5 degrees angle of attack. As with the Mach 0.95 results, vortical flow exists near the leading edge at the 10, 30, and 60% span stations. Here, the vortical flow regions are more localized than in the Mach 0.95 results and the correlation is generally better, particularly at 60% span.

In a previous section it was stated that the tendency of the lower surface to generate vortical flows inboard at moderate negative angles of attack might be a contributing factor to the unusual flutter boundary presented in figure 7. This characteristic appears to be supported by the present analyses where vortical flow is predicted on the inboard sections of the wing at α_o= -3 and -5 degrees but not at α_o= 3 and 6 degrees.

Unsteady Computational Results and Comparisons with Experimental Data

Sinusoidal unsteady pitching calculations were performed at Mach numbers 0.5 and 0.95 with α_o=6, 3, -3, and -5 degrees. As rigid body motion is being simulated, the rigid grid rotation feature in CFL3D was used. Here, the entire grid rotates with the wing at the specified amplitude and frequency. The pitch rotation point was the same as the wind-tunnel model, the frequency used in these unsteady analyses was 5 Hz. and the amplitude of oscillation was 1 degree. The 5 Hz. frequency was selected because it is close to the RSM/PAPA flutter frequency, and the objective of this work is aeroelastic analysis. Finally, grid 2 was used in all the unsteady calculations.

These unsteady calculations use the steady solutions described in the previous section of the paper as a starting point. Most calculations were performed with 200 time steps per cycle and 15 subiterations per time step. This resulted in a drop of over 2.5 orders of magnitude in the residual at each time step. To verify a satisfactory solution was being obtained, a 400 time step per cycle case was run with no difference noted in the solution. A minimum of four cycles of oscillation were calculated in each case (M and α_o combination). The fourth cycle was compared with previous cycles to verify that periodic behavior of the flow had converged. The same discrete Fourier transform procedure previously applied to the experimental time history data was used to reduce the final, converged cycle of the CFL3D results.

The correlation between unsteady experimental data and CFL3D results varied greatly depending on angle of attack, span station, and Mach number. The correlation on the pressure side of the wing was generally good for subsonic cases and to a lesser extent for the transonic cases. Another general observation was that when key flow features could be identified on the steady experimental data and those features were captured by CFL3D, the correlation was generally consistent. However, in the absence of key flow features like obvious vortical flow in steady data, the unsteady correlation was generally very poor even when the steady correlation looked good. One final general observation was that the suction side correlation was always poor at 95% span.

Figures 12 and 13 provide a comparison between unsteady experimental data and CFL3D results for Mach numbers 0.5 and 0.95, respectively, both at -5 degrees angle of attack. The effects of vortex motion can be seen at 10, 30, and 60% span stations for both the experimental data and the CFL3D results. Vortex amplitude and location is more accurately predicted in the subsonic case. As with the steady data, the effects of the vortex tends to be generally smeared as compared with the experimental data. At 95% span the correlation is only satisfactory on the pressure side in the subsonic case.

Future research involving this wind-tunnel model and data set will focus on the computational analysis of the highly-nonlinear flutter boundaries shown in figure 7. A computationally-efficient reduced-order modeling (ROM) approach[19] is currently being applied to this problem. This ROM approach enables the creation of linearized, unsteady aerodynamic models about nonlinear steady-state flow conditions using CFD-based responses. These linearized, unsteady aerodynamic models are then coupled with models of the structure in order to rapidly generate aeroelastic transients at any dynamic pressure of interest without re-execution of the CFD code. Hong[20] successfully applied this method to unsteady aerodynamic responses of the RSM and to flutter analysis of a Boeing transport aircraft. Application of this ROM methodology will provide valuable insight regarding the influence of a nonlinear steady-state flow condition (shock, vortex) on the unsteady aerodynamic response of a vehicle, including flutter.

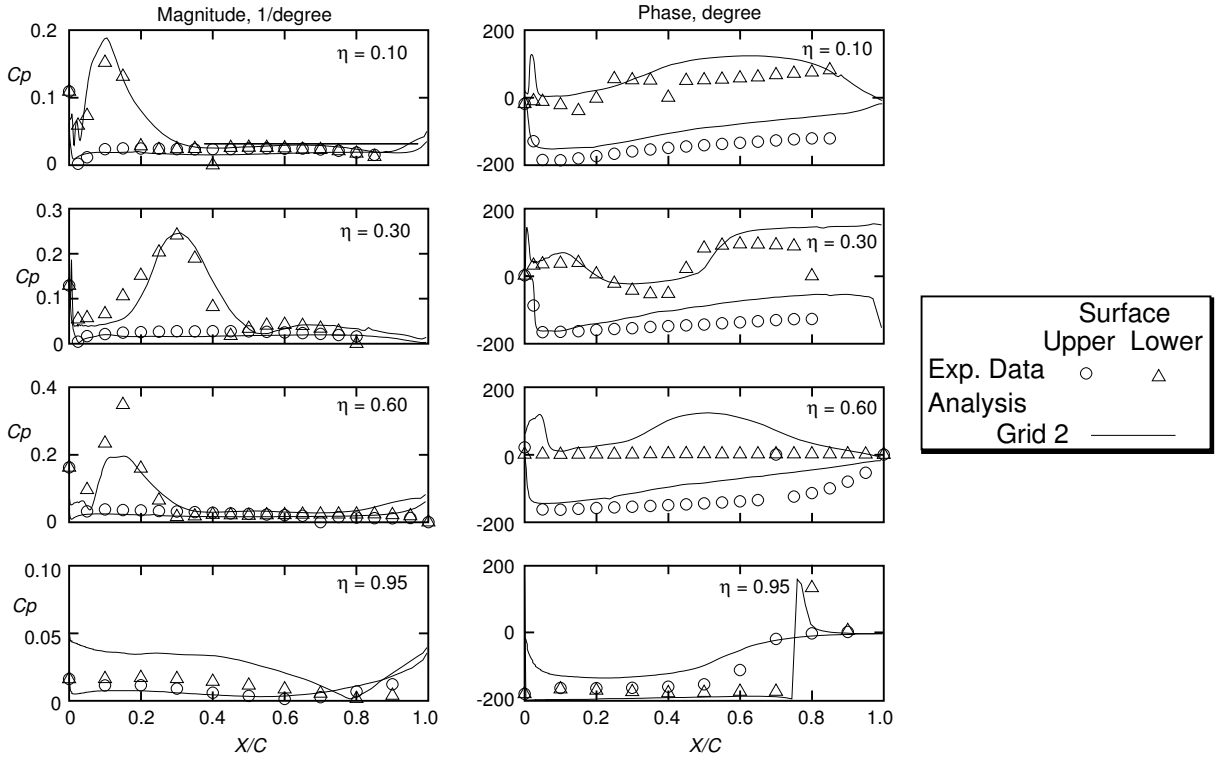

Fig. 12 Comparison of CFL3D analysis and Test 547 (RSM/OTT) unsteady pressure coefficients. M=0.5, q=150 psf, Re=4.3$\times 10^6$/ft, f=5 Hz., α_o=-5 deg., α_1=±1 deg.

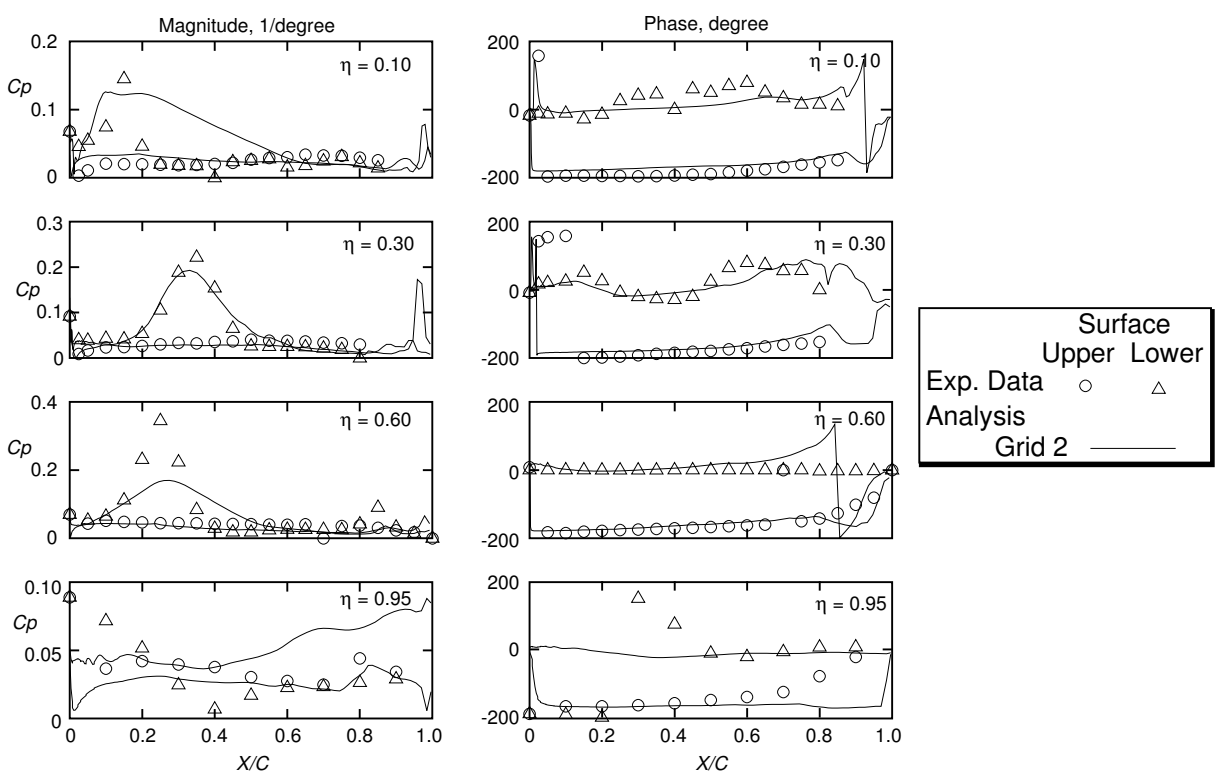

Fig. 13 Comparison of CFL3D analysis and Test 547 (RSM/OTT) unsteady pressure coefficients. M=0.95, q=150 psf, Re=2.2$\times 10^6$/ft, f=5 Hz., and α_o=-5 deg., α_1=±1 deg.

Concluding Remarks

A large database of steady, unsteady, and flutter wind-tunnel data has been obtained for three configurations based on an HSCT design: the Rigid Semispan Model (RSM) on a balance, the RSM on a Pitch and Plunge Apparatus (PAPA), and the RSM on the Oscillating Turntable (OTT). The database covers an extensive Mach number range from subsonic to low supersonic with a special focus on transonic conditions. The RSM was highly instrumented and the acquired database represents one of the largest aerodynamic and aeroelastic databases available. Examples of steady and unsteady pressure data were shown. The flutter behavior of the RSM on the PAPA mount was examined. Steady and unsteady CFD analyses were performed and compared with experimental data. Correlation for the steady cases was generally good, with some difficulty in fully capturing the vortical flow noted. Correlation for the unsteady pitch oscillation cases varied greatly with flow conditions and span station with the subsonic cases providing better correlation than the transonic ones.

Acknowledgements

The authors would like to acknowledge the support of Mr. Norm Willey for acquiring the photogrammetry data and the support of Mr. Carl Rogers of in generating the RSM grids.

References

[1]Ruiz-Calavera, L. P. and et al, "A New Compendium of Unsteady Aerodynamic Test Cases for CFD: Summary of AVT WG-003 Activities," *International Forum on Aeroelasticity and Structural Dynamics*, June 1999.

[2]Bennett, R. M., Eckstrom, C. V., Rivera, Jr, J. A., Dansberry, B. E., Farmer, M. G., and Durham, M. H., "The Benchmark Aeroelastic Models Program: Description and Highlights of Initial Results," NASA TM 104180, April 1991.

[3]Durham, M. H., Keller, D. F., Bennett, R. M., and Wieseman, C. D., "A Status Report on a Model for Benchmark Active Controls Testing," *AIAA/ASME/ASCE/AHS/ASC 32nd Structures, Structural Dynamics, and Materials Conference*, No. 91-1011, Baltimore, MD, April 1991.

[4]Rivera, Jr, J. A., Dansberry, B. E., Bennett, R. M., Durham, M. H., and Silva, W. A., "NACA0012 Benchmark Model Experimental Flutter Results with Unsteady Pressure Distributions," NASA TM 107581, April 1992.

[5]Rivera, Jr, J. A., Dansberry, B. E., Durham, M. H., Bennett, R. M., and Silva, W. A., "Pressure Measurements on a Rectangular Wing with a NACA0012 Airfoil During Conventional Flutter," NASA TM 104211, July 1992.

[6]Dansberry, B. E., Durham, M. H., Bennett, R. M., Turnock, D. L., Silva, W. A., and Rivera Jr, J. A., "Physical Properties of the Benchmark Models Program Supercritical Wing," NASA TM 4457, Sept. 1993.

[7]Scott, R. C., Hoadley, S. T., Wieseman, C. D., and Durham, M. H., "The Benchmark Active Controls Technology Model Aerodynamic Data," *Proceedings of the 35th Aerospace Sciences Meeting and Exhibit*, No. 97-0829, Reno, NV, Jan. 1997.

[8]Schuster, D. M., Spain, C. V., and et al, "Development, Analysis, and Testing of the High Speed Research Flexible Semispan Model," NASA CR 1999-209556, Sept. 1999.

[9]Scott, R. C., Silva, W. A., Florance, J. R., and Keller, D. F., "Measurement of Unsteady Pressure Data on a Large HSCT Semispan Wing and Comparison with Analysis," *AIAA/ASME/ASCE/AHS/ASC 43rd Structures, Structural Dynamics, and Materials Conference*, No. 2002-1648, April 2002.

[10]Corliss, J. M. and Cole, S. R., "Heavy Gas Conversion of the NASA Langley Transonic Dynamics Tunnel," *Proceedings of the 20th Advanced Measurements and Ground Testing Technology Conference*, No. 98-2710, Albuquerque, NM, June 1998.

[11]Cole, S. R. and Rivera Jr, J. A., "The New Heavy Gas Testing Capability in the NASA Langley Transonic Dynamics Tunnel," *Royal Aeronautical Society Wind Tunnels and Wind Tunnel Test Techniques Forum*, No. 4, Cambridge, UK, April 1997.

[12]Farmer, M. G., "A Two-Degree-of-Freedom Flutter Mount System with Low Damping for Testing Rigid Wings at Different Angles of Attack," NASA TM 83302, 1982.

[13]Silva, W. A., Keller, D. F., Florance, J. R., Cole, S. R., and Scott, R. C., "Experimental Steady and Unsteady Aerodynamic and Flutter Results for HSCT Semispan Models," *AIAA/ASME/ASCE/AHS/ASC 41st Structures, Structural Dynamics, and Materials Conference*, No. 2000-1697, April 2000.

[14]Piatak, D. J. and Cleckner, C. S., "A New Forced Oscillation Capability for the Transonic Dynamics Tunnel," *40th Aerospace Sciences Meeting and Exhibit*, Reno, NV, Jan. 2002.

[15]Schuster, D. M. and Rausch, R. D., "Transonic Dynamics Tunnel Force and Pressure Data Acquired on the HSR Rigid Semispan Model," NASA CR 1999-209555, Sept. 1999.

[16]Kris, S. L., Biedron, R. T., and Rumsey, C. L., "CFL3D User's Manual Version 5.0," NASA-TM 1998-208444, NASA Langley Research Center, Hampton, VA, June 1998.

[17]Bartels, R. E. and Biedron, R. T., "CFL3D Version 6.0 User's Manual for Aeroelastic and Deforming mech Simulation," Unpublished, NASA Langley Research Center, Hampton, VA.

[18]Bartels, R. E. and Gatski, T. B., "Prediction of Transonic Vortex Flows Using Linear and Nonlinear Turbulent Eddy Viscosity Models," NASA-TM 2000-210282, May 2000.

[19]Silva, W. A. and Bartels, R. E., "Development of Reduced-Order Models for Aeroelastic Analysis and Flutter Prediction Using the CFL3Dv6.0 Code," *Proceedings of the 43rd AIAA/ASME/ASCE/AHS/ASC Structures, Structural Dynamics and Materials Conference*, No. 02-1596, Denver, CO, April 2002.

[20]Hong, M. S., Kuruvila, G., Bhatia, K. G., Sen-Gupta, G., and Kim, T., "Evaluation of CFL3D for Unsteady Pressure and Flutter Predictions," *AIAA/ASME/ASCE/AHS/ASC 44rd Structures, Structural Dynamics, and Materials Conference*, No. 2003-1932, April 2003.